International Journal of Mass Spectrometry 308 (2011) 109–113

Contents lists available at ScienceDirect

International Journal of Mass Spectrometry

journal homepage: www.elsevier.com/locate/ijms

Numerical investigation of stability regions in a cylindrical ion trap

Houshyar Noshad [a,*], Behjat-Sadat Kariman [b]

[a] Department of Nuclear Engineering and Physics, Amirkabir University of Technology (Tehran Polytechnic), P.O. Box 15875-4413, Hafez Avenue, Tehran, Iran
[b] Plasma Physics Research Center, Science and Research Branch, Islamic Azad University, Tehran, Iran

ARTICLE INFO

Article history:
Received 10 May 2011
Received in revised form 2 August 2011
Accepted 3 August 2011
Available online 10 August 2011

Keywords:
Cylindrical ion trap
Stability regions
Fifth-order Runge–Kutta method
Sixth-order Runge–Kutta method with step-size control
Power regression
Stability region areas

ABSTRACT

Numerical computation of the equations governing the behavior of an ion in a cylindrical ion trap (CIT) was carried out using an algorithm based on the fifth-order Runge–Kutta (RK5) method. Afterwards, three stability regions for the CIT were computed via combination of the RK5 method and sixth-order Runge–Kutta (RK6) method with step-size control. The first region is in good agreement with the previous result in the literature, whereas the second and third stability regions obtained in this work are reported for the first time using the RK5 and RK6 methods. As a new conclusion, we demonstrated that the ratio of areas of the stability region for the CIT to that of a quadrupole ion trap (QIT) is the same for the three regions. Moreover, dependence of stability regions of the CIT on the trap dimensions as well as initial conditions of ions were investigated. We concluded that for the first region, the maximum value of q when $U=0$, namely q_{max}, follows a power regression function, which has not been reported previously.

1. Introduction

Today's, ion traps with various geometries are used for storage of charged particles. Among these geometries, traps with hyperbolic ring and end-cap electrodes, the so-called Paul traps (QIT), are widely used in research and industries due to its ability to do multistage MS/MS experiments as well as its simple mathematical description [1]. The simplicity is mainly attributed to the quadrupole electric field into the trap, which results the classified mathematical formalism known as the Mathieu equation [2]. Because of these, there are a lot of articles published concerning the characteristics of Paul traps [3–6]. It is worth noting that, ion traps with cylindrical shape have also received special attention of the research groups due to some advantages [7–10]. Among them, one can mention much easier construction of the CIT in comparison with the Paul trap [8], which enables us to utilize a cylindrical ion trap for miniaturization [9,11]. Although the CIT has a simple geometry for fabrication, its mathematical description is more difficult than that of a Paul trap [12].

For some specialized applications of mass spectrometry, a mass filter or an ion trap is designed to operate in higher stability regions instead of the first region [3]. It should be noted that the range of mass-to-charge ratio for the ions that can be stored in the higher stability regions of three-dimensional traps is very low. Perhaps this is why they are rarely used, at least for analytical mass spectrometry. One can find some articles deal with mass spectrometry of light ions with the energies of the order of several keV using the quadrupole mass filters operating in higher stability regions [13]. Regarding high-resolution mass spectrometry, it should be noted that it would be probably going too far to call the QIT a high-resolution mass spectrometer. Hence, mass filters are usually applied for higher resolutions. For instance, higher resolution spectrometry was used to separate atomic ions from molecular ions, which differ in mass by up to 1 part in 2500 [14]. The high-resolution mass spectrometry was experimentally demonstrated by means of a quadrupole mass filter operated in the second region of stability [14] with Mathieu parameters $(a, \nleftrightarrow q) \approx (0.03, \nleftrightarrow 7.55)$, which was sufficient to resolve some atomic ions from molecular ions. As another experimental evidence, one can mention operation of a mass filter in the third stability region [15] with $(a, \nleftrightarrow q) \approx (3, \nleftrightarrow 3)$, which allowed mass analysis with higher resolutions. Moreover, a resolution of several thousands was obtained with ions of several thousand eV energy using a mass filter operated in the fourth stability region [16] with Mathieu parameters $(a, \nleftrightarrow q) = (2 \times 10^{-3}, \nleftrightarrow 21.3)$.

The objective of this article is to study the dynamical behavior of charged particles in a cylindrical ion trap as well as computation of its three stability regions using the fifth-order Runge–Kutta method [17]. Special care was taken to make the computation of the points at the corner of the regions to be carried out accurately. For this purpose, the sixth-order Runge–Kutta method with step-size control [18] was used. The first region of stability obtained from this work is satisfactorily consistent with the corresponding region found in the literature [7]. Notably, the second and third stability

* Corresponding author. Tel.: +98 912 2216322; fax: +98 21 66495519.
E-mail address: hnoshad@aut.ac.ir (H. Noshad).

1387-3806/$ – see front matter © 2011 Elsevier B.V. All rights reserved.
doi:10.1016/j.ijms.2011.08.007

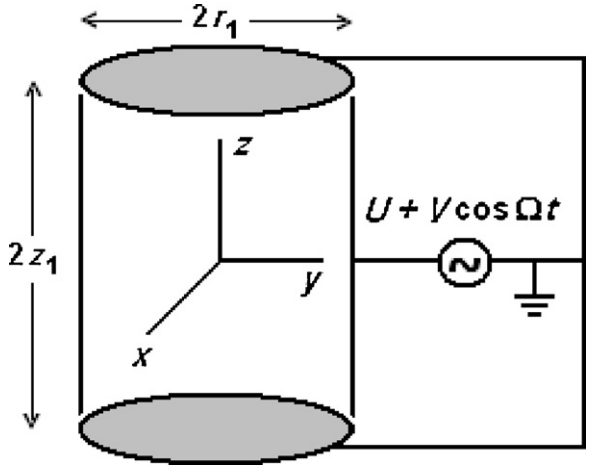

Fig. 1. A schematic view of a cylindrical ion trap.

regions computed for the CIT have not been reported in the literature previously using the RK5 and RK6 methods. Furthermore, the dependence of the stability regions on the trap sizes as well as on the initial conditions of ions was investigated.

2. Theoretical description

Fig. 1 shows a schematic view of a cylindrical ion trap with grounded end-cap electrodes. Applying electric potential $\varphi_0 = U + V\cos\,\Omega t$ to the ring electrode, the potential distribution into the CIT is given by solving the Laplace's partial differential equation in cylindrical coordinates [19]. In the relation, U and V are dc and zero-to-peak ac voltages, respectively, whereas Ω denotes the angular frequency of the rf signal in rad/s. Although the numerical study of the CIT is rather more complicated in comparison with a Paul trap, the mathematical derivation of the formulas is straightforward, and can be found in the literature [7,8,20]. The potential into the cylindrical ion trap can be written as [7]

$$\varphi(r,z) = \sum_{n=0}^{\infty} \frac{4(-1)^n (U + V\cos\,\Omega t)}{(2n+1)\pi I_0(l_n r_1)} I_0(l_n r)\cos(l_n z), \tag{1}$$

where I_0 stands for the 0th-order modified Bessel function of the first kind, and l_n is defined by

$$l_n = \frac{(2n+1)\pi}{2z_1} \qquad n = 0, 1, 2, \ldots \tag{2}$$

Applying $E = -\nabla\varphi$, the electric field components into the CIT are expressed by

$$E_r = -\frac{2(U + V\,\cos\,\Omega t)}{z_1} \sum_{n=0}^{\infty} \frac{(-1)^n}{I_0(l_n r_1)} I_1(l_n r)\cos(l_n z) \tag{3}$$

$$E_z = \frac{2(U + V\,\cos\,\Omega t)}{z_1} \sum_{n=0}^{\infty} \frac{(-1)^n}{I_0(l_n r_1)} I_0(l_n r)\sin(l_n z), \tag{4}$$

where I_1 denotes the first-order modified Bessel function of the first kind. The r and z positions of a particle of mass M and electric charge Q into the CIT are given as follows:

$$\frac{d^2 r}{dt^2} = -\frac{2Q(U + V\,\cos\,\Omega t)}{Mz_1} \sum_{n=0}^{\infty} \frac{(-1)^n}{I_0(l_n r_1)} I_1(l_n r)\cos(l_n z) \tag{5}$$

$$\frac{d^2 z}{dt^2} = \frac{2Q(U + V\,\cos\,\Omega t)}{Mz_1} \sum_{n=0}^{\infty} \frac{(-1)^n}{I_0(l_n r_1)} I_0(l_n r)\sin(l_n z). \tag{6}$$

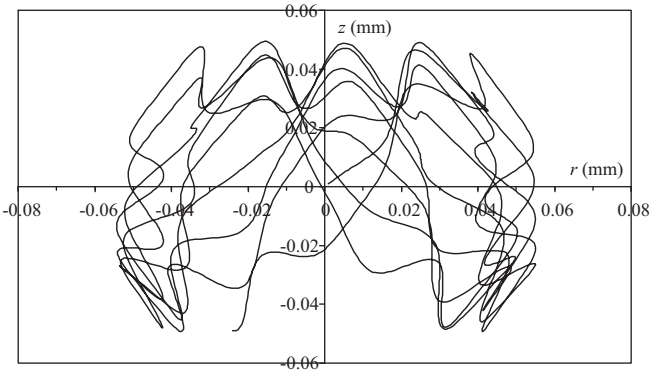

Fig. 2. The trajectories of an H^+ ion for $r_1 = 2.5$ mm, $z_1 = 2.88$ mm, $f = 1$ MHz, $U = 0$ and $V = 100$ V, and hence $\alpha_z = 0$ and $\xi_z = 233.7$.

Eqs. (5) and (6) are transformed to the following set of coupled differential equations

$$\frac{d^2 r}{d\tau^2} + (\alpha_r - 2\xi_r\,\cos 2\tau) f(r,z) = 0 \tag{7}$$

$$\frac{d^2 z}{d\tau^2} + (\alpha_z - 2\xi_z\,\cos 2\tau) g(r,z) = 0, \tag{8}$$

where $f(r,z)$ and $g(r,z)$ are defined by

$$f(r,z) = z_1 \sum_{n=0}^{\infty} \frac{(-1)^n I_1(rl_n)\cos(zl_n)}{I_0(r_1 l_n)} \tag{9}$$

$$g(r,z) = \frac{z_1}{2} \sum_{n=0}^{\infty} \frac{(-1)^n I_0(rl_n)\sin(zl_n)}{I_0(r_1 l_n)}, \tag{10}$$

respectively. The dimensionless parameters α_z, α_r, ξ_z, ξ_r and τ in Eqs. (7) and (8) are given by

$$\alpha_z = -2\alpha_r = \frac{-16QU}{Mz_1^2\Omega^2} \tag{11}$$

$$\xi_z = -2\xi_r = \frac{8QV}{Mz_1^2\Omega^2} \tag{12}$$

$$\tau = \frac{\Omega t}{2}. \tag{13}$$

3. Results and discussion

The set of coupled ordinary differential Eqs. (7) and (8) was numerically solved by using the fifth-order Runge–Kutta (RK5) method. This method and the mathematical algorithm can be found in detail in Ref. [17]. Fig. 2 depicts the trajectories for a typical ion such as H^+ confined in the CIT with $r_1 = 2.5$ mm, $z_1 = 2.88$ mm, $f = 1$ MHz, $U = 0$ and $V = 100$ V, which shows the stable dynamical behavior of the ion. For these quantities, the corresponding values of 0 and 233.7 were obtained for α_z and ξ_z, respectively. In this computation, we used ion positions of 1×10^{-6} mm for both r and z components as initial positions, whereas the initial ion velocities were selected as zero for the two components. It is worthwhile to note that for an ideal Paul trap, the type of ion motion, and hence the motional stability is independent of the initial position and velocities of the ions. This is no longer true if nonlinear fields are included as is the case for the CIT. The stability region of a nonlinear trap such as the CIT hence also depends on the initial spatial and velocity coordinates. In other words, the results obtained will depend on the chosen initial conditions. In this analysis, we selected the simple initial conditions of 0 and 1×10^{-6} mm for ion velocities and position, respectively. In fact, first, we were interested in choosing 0 for

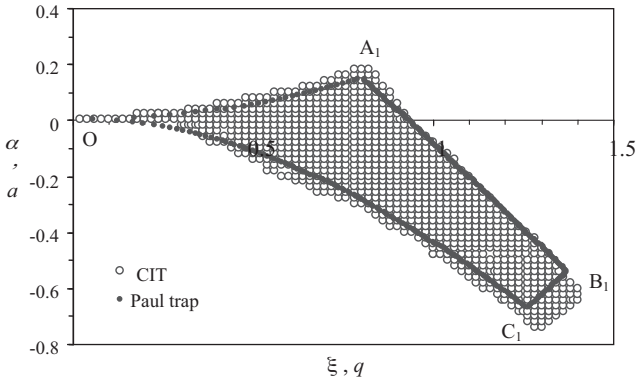

Fig. 3. The first stability regions for the CIT and the Paul trap. The open circles correspond to our computation for the CIT with $r_1 = 2.5$ mm and $z_1 = 2.88$ mm; whereas, the black circles represent the corresponding data for a Paul trap taken from Ref. [3].

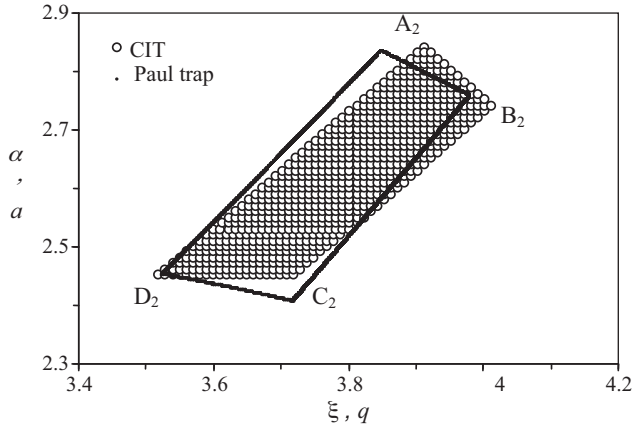

Fig. 4. The second stability regions for the CIT and the Paul trap. The open circles correspond to our computation for the CIT with $r_1 = 2.5$ mm and $z_1 = 2.88$ mm; whereas, the black circles represent the corresponding data for a Paul trap taken from Ref. [3].

the initial ion position. But under these conditions, due to the symmetry, no motions of ions were observed in our simulation. Hence, we selected the initial position to be as 1×10^{-6} mm instead of zero. The other reason for selecting 1×10^{-6} mm was that it enabled us to compare our first stability region with the corresponding region reported by Lee [7].

The three stability regions for the CIT with $r_1 = 2.5$ mm and $z_1 = 2.88$ mm with initial ion position of 1×10^{-6} mm are shown in Figs. 3–5. Reassuringly, the points at the corners of the regions were computed using the RK6 method with step-size control [18] as well. This method is based on a complete coverage of the leading local truncation error term, which is similar to the classical Runge–Kutta formulas without step-size control. The formulas obtained from the RK6 method with step-size control has an advantage over the other methods. These formulas contain one or more parameters, which by a proper choice of them, the leading term of the local truncation

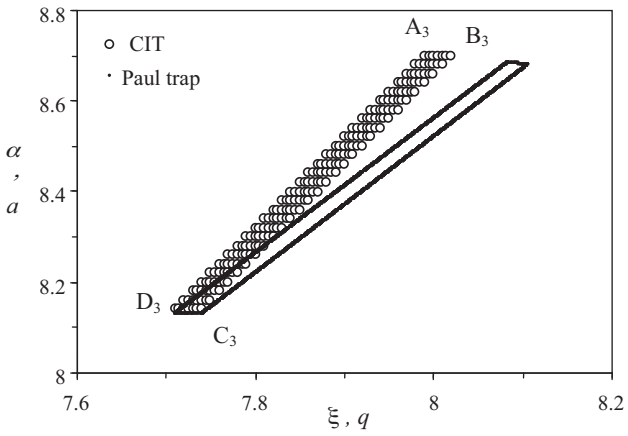

Fig. 5. The third stability regions for the CIT and the Paul trap. The open circles correspond to our computation for the CIT with $r_1 = 2.5$ mm and $z_1 = 2.88$ mm; whereas, the black circles represent the corresponding data for a Paul trap taken from Ref. [3].

error reduces substantially. This, in general, results in an increase of the permissible step-size and, as a consequence, smaller number of evaluations per step [18]. In other words, in this method, we save the steps since the local truncation error is smaller. In our computation, the number of steps was selected as 3450. Hence, by considering 10th number of evaluations per step, the total number of evaluations in our simulation was 34,500.

In Figs. 3–5, the corresponding results for a Paul trap taken from Noshad and Doroudi [3] are also included in order to be able to compare our results for the CIT with them at a glance. Table 1 shows the values of α and ξ at the corners of the three stability regions for the cylindrical ion trap as well as the values of a and q at the corners of the corresponding regions for the conventional Paul trap.

It is notable that area of a stability region is frequently used as an appropriate parameter, which enables us to compare two regions with each other properly [21]. For this purpose, the ratio of areas of stability regions can be used as well. In this work, we computed the points of the first stability region for the CIT by using the RK5 method [17], and good agreements were found between the area calculated for our first region and that of published by Lee [7]. In our computational approach, the parameters α and ξ were scanned until a trajectory was found to be stable. To verify that for a given α and ξ the set of Eqs. (7) and (8) has stable solutions, the computations were made for 300 rf cycles in the ion trajectory. To determine the step sizes for α and ξ parameters, a compromise between the required accuracy and time allotted for the computation is needed. Smaller step sizes give slower computation but higher accuracy, whereas larger steps result faster computation and less accuracy. In this computation, step sizes for α parameter were selected as 0.02, 0.01 and 0.02, while for ξ parameter the steps were considered as 0.02, 0.01 and 0.005 for the first, second and the third regions, respectively. By considering these values for α and ξ, an optimization for the accuracy was made. Under these conditions, the uncertainty of 2.1% was obtained for computation of our first stability region as compared to the corresponding region published

Table 1
The values of α and ξ for the points at the corners of the stability regions of the CIT computed in this work as well as the corresponding values of a and q for a QIT.

		First stability region				Second stability region				Third stability region			
		A_1	B_1	C_1	O	A_2	B_2	C_2	D_2	A_3	B_3	C_3	D_3
CIT	α	0.18	−0.64	−0.74	0	2.84	2.74	2.46	2.45	8.70	8.71	8.14	8.14
	ξ	0.78	1.40	1.30	0	3.91	4.01	3.72	3.52	7.99	8.02	7.75	7.71
QIT	aa	0.15	−0.53	−0.67	0	2.84	2.76	2.41	2.45	8.69	8.68	8.13	8.13
	qq	0.79	1.35	1.23	0	3.85	3.98	3.72	3.52	8.08	8.11	7.74	7.71

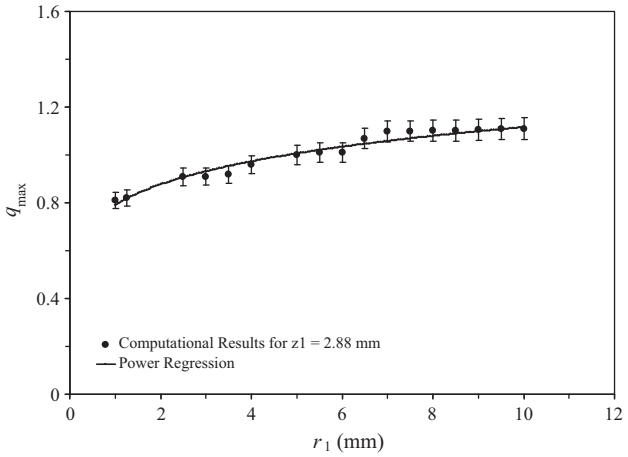

Fig. 6. q_{max} as a function of r_1 for the first stability region of a cylindrical ion trap with z_1 = 2.88 mm and the power regression.

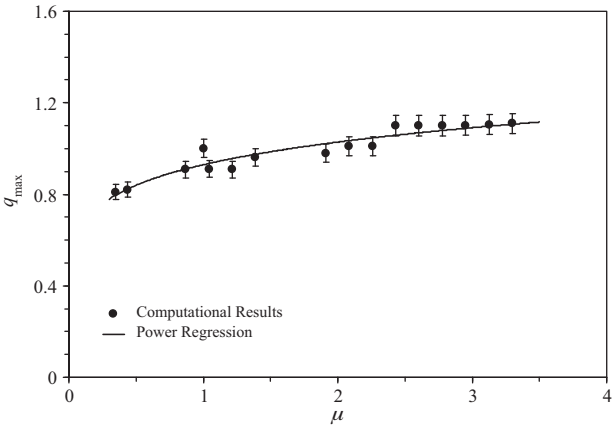

Fig. 8. q_{max} as a function of $\mu = r_1/z_1$ for the first stability region of a cylindrical ion trap and the power regression.

by Lee [7]. For the second and third regions, error propagation formula [22] gives an average uncertainty of 1.8%. It should be noted that as far as we know, no article has been published regarding the second and third regions of stability for a cylindrical ion trap using RK5 and RK6 methods. Furthermore, the areas of the three stability regions for a CIT with r_1 = 2.5 mm and z_1 = 2.88 mm as well as for a Paul trap were evaluated. We drew a conclusion that the ratio of the areas for the CIT to the corresponding value of a QIT, namely S_{CIT}/S_{QIT}, is the same for the first, second and third stability regions. Similar computations were also made for another values of r_1 and z_1, and our conclusion was confirmed. In the case of r_1 = 2.5 mm and z_1 = 2.88 mm, this ratio was calculated to be as $1.23 \overleftrightarrows \pm \overleftrightarrows 0.03$.

The effect of the trap dimensions, namely $r_1 \overleftrightarrows$ and z_1, on the first stability region was investigated by computation of the maximum value of q when U = 0, namely q_{max}. Figs. 6 and 7 show q_{max} versus r_1 and z_1, respectively. One can see that q_{max} can be properly explained by a function based upon the least square method, which slightly increases as the dimension of the trap increases. A nonlinear fitting gives appropriate power regression functions presented by Eqs. (14) and (15) for z_1 = 2.88 mm and r_1 = 2.5 mm, respectively. In addition, similar evaluation for q_{max} versus $\mu = r_1/z_1$ can be seen in Fig. 8, and the corresponding power regression function is shown by Eq. (16). In Figs. 6–8 the fitted curves are able to reproduce the computational data within the uncertainty of 4% using the error propagation formula [22].

$$q_{max} = 0.79 \overleftrightarrows r_1^{0.15} \tag{14}$$

$$q_{max} = 0.77 \overleftrightarrows z_1^{0.21} \tag{15}$$

$$q_{max} = 0.93 \mu^{0.15} \tag{16}$$

The similar curve fittings were also made for other values of $r_1 \overleftrightarrows$ and z_1, and consequently power regression function of the form $q_{max} = a \overleftrightarrows w^b$ was demonstrated, where a and b are constants, and $\overleftrightarrows w$ stands for r_1, z_1 or μ.

Furthermore, the computation was carried out for the second region of a CIT with twofold in dimensions in order to investigate the influence of r_1 and z_1 on the stability diagram. Fig. 9 shows the second region of stability for r_1 = 5 mm and z_1 = 5.76 mm as well as the corresponding region for r_1 = 2.5 mm and z_1 = 2.88 mm. To confirm that the discordance of the stability region is significant and is not related to the error of the computational technique, we used the sixth-order Runge–Kutta method with step-size control as well. One can see that the region is enlarged for a double-sized cylindrical ion trap. It means that the calculation of the second stability region is also sensitive to the dimensions of an ion trap with a cylindrical shape. In other words, stability regions of the CIT depend on the trap sizes. This conclusion is supported, on the one hand, by the results published in Ref. [23] and, on the other hand, by Eqs. (7) and (8) in which the parameters α_z, α_r, ξ_z and ξ_r as well as two

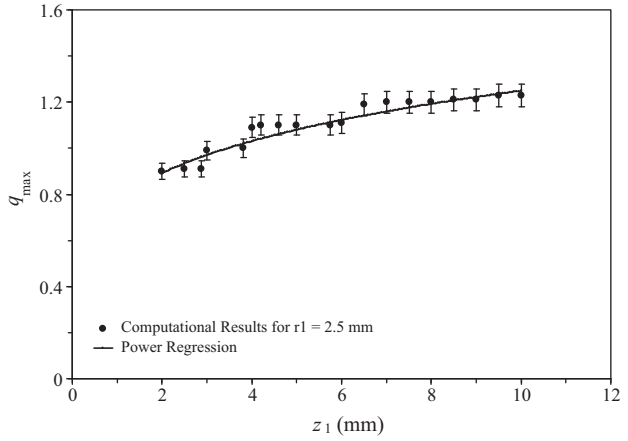

Fig. 7. q_{max} as a function of z_1 for the first stability region of a cylindrical ion trap with r_1 = 2.5 mm and the power regression.

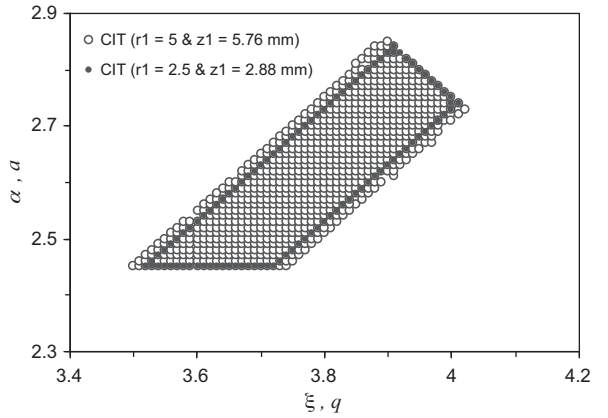

Fig. 9. The second stability regions for the CIT with two different dimensions. The open circles correspond to the double-sized CIT, whereas the black ones represent the second region as depicted in Fig. 4.

nonlinear terms $f(r, z)$ and $g(r, z)$ are functions of trap dimensions, namely r_1 and z_1.

To investigate the dependence of stability regions on initial conditions, we computed q_{max} for $r_1 = 2.5$ mm, $z_1 = 2.88$ mm. In this computation, the initial ion velocity was considered to be 0, whereas the initial positions of ions were assumed to be equal to various values. As a result, we observed variations of q_{max} and hence changes in the stability regions, if the selected initial spatial coordinates of ions (r_0, z_0) are not too small compared to typical dimensions of the ion cloud (FWHM of about 1 mm). For instance, by considering $(r_0, z_0) = (0.1, 0.1)$ mm and also $(r_0, z_0) = (1, 1)$ mm, the results differ with each other more significantly. Furthermore, we drew a conclusion that in order to obtain the same results for a single- and double-sized CIT, the initial positions need to be scaled by the same factor as the trap size. As a numerical evaluation, our computation showed that for a CIT with $r_1 = 2.5$ mm, $z_1 = 2.88$ mm and initial positions $(r_0, z_0) = (0.1, 0.1)$ mm, the stability regions are the same as for a double-sized CIT, namely $r_1 = 5$ mm, $z_1 = 5.76$ mm and initial positions of $(r_0, z_0) = (0.2, 0.2)$ mm. This fact can also explain the different stability regions found in our computation for a single- and double-sized cylindrical ion trap with the same initial ion positions as shown in Fig. 9.

4. Conclusions

The motion of ions in a cylindrical ion trap as well as the three regions of stability were numerically investigated. Computation of the stability regions in an ion trap such as a CIT requires high-accuracy numerical techniques. It is worth noting that the RK5 method can be considered as an appropriate and accurate-enough technique. Nonetheless, the points at the corners of the regions were recomputed by using the sixth-order Runge–Kutta method with step-size control. One can see that the first stability region of the CIT is similar to that of the Paul trap except for some negative values of dc voltages, for which an expansion is observed. Moreover, the second and third regions of the CIT are in discord with those of the Paul trap. The discordance is more apparent in comparison with the first stability region.

Evaluation of the ratio of the area for the stability regions of a CIT to the corresponding region of a Paul trap shows that the ratio is the same for the three regions of stability. For a CIT with $r_1 = 2.5$ mm and $z_1 = 2.88$ mm, the ratio was calculated to be as $1.23 \rightleftarrows \pm \rightleftarrows 0.03$.

We drew a conclusion that the stability regions for the CIT depend on the dimensions of the trap, whereas for the Paul trap does not. Furthermore, it is demonstrated that q_{max} as a function of the trap dimensions can be properly explained by a power regression function, which has not been investigated previously. Moreover, our results confirm that for a cylindrical ion trap, the stability regions depend on the trap dimensions as well as ion initial conditions, contrary to the case of a Paul trap.

References

[1] P.H. Dawson, Quadrupole Mass Spectrometry and its Applications, AIP, New York, 1995, p. 69.
[2] M. Abramowitz, I.A. Stegun, Handbook of Mathematical Functions, Dover Publishing, New York, 1972, p. 721.
[3] H. Noshad, A. Doroudi, Computation of five stability regions in a quadrupole ion trap using the fifth-order Runge–Kutta method, Int. J. Mass Spectrom. 281 (2009) 79–81.
[4] I. Ziaeian, H. Noshad, Theoretical study of the effect of damping force on higher stability regions in a Paul trap, Int. J. Mass Spectrom. 289 (2010) 1–5.
[5] X. Zhu, D. Qi, Characteristics of trapped ions in the second stability region of a Paul trap, J. Mod. Opt. 39 (1992) 291–303.
[6] W. Jiebing, Z. Xiwen, Phase space analysis of the ion cloud in the second stability region of the Paul trap, Int. J. Mass Spectrom. Ion Processes 124 (1993) 89–97.
[7] W.W. Lee, C.H. Oh, P.S. Kim, M. Yang, K. Song, Characteristics of cylindrical ion trap, Int. J. Mass Spectrom. 230 (2003) 25–31.
[8] R.F. Bonner, J.E. Fulford, R.E. March, The cylindrical ion trap. Part I. General introduction, Int. J. Mass Spectrom. Ion Phys. 24 (1977) 255–269.
[9] E.R. Badman, R.C. Johnson, W.R. Plass, R.G. Cooks, A miniature cylindrical quadrupole ion trap: simulation and experiment, Anal. Chem. 70 (1998) 4896–4901.
[10] J.M. Wells, E.R. Badman, R.G. Cooks, A quadrupole ion trap with cylindrical geometry operated in the mass-selective instability mode, Anal. Chem. 70 (1998) 438–444.
[11] C. Champenois, M. Knoop, M. Herbane, M. Houssin, T. Kaing, M. Vedel, F. Vedel, Characterization of a miniature Paul–Straubel trap, Eur. Phys. J. D 15 (2001) 105–111.
[12] R.F. Bonner, J.E. Fulford, R.E. March, G.F. Hamilton, The cylindrical ion trap. Part 1. General introduction, Int. J. Mass Spectrom. Ion Phys. 24 (1977) 255–269.
[13] L. Moens, N. Jakubowski, Double-focusing mass spectrometers in ICPMS, Anal. Chem. 70 (1998) 251A–256A.
[14] J.F. Ying, D.J. Douglas, High resolution inductively coupled plasma mass spectra with a quadrupole mass filter, Rapid Commun. Mass Spectrom. 10 (1996) 649–652.
[15] Z. Du, T.N. Olney, D.J. Douglas, Inductively coupled plasma mass spectrometry with a quadrupole mass filter operated in the third stability region, J. Am. Soc. Mass. Spectrom. 8 (1997) 1230–1236.
[16] W. Chen, B.A. Collings, D.J. Douglas, High-resolution mass spectrometry with a quadrupole operated in the fourth stability region, Anal. Chem. 72 (2000) 540–545.
[17] D. Goeken, O. Johnson, in: 15th Annual Conference of Applied Mathematics, Univ. of Central Oklahoma, Electronic Journal of Differential Equations, Conference 02 (1999) 4–5.
[18] E. Fehlberg, Classical fifth-, sixth-, seventh-, and eighth-order Runge–Kutta formulas with stepsize control, NASA Technical Report TR R-287, 1968.
[19] J.D. Jackson, Classical Electrodynamics, third ed., Wiley, New York, 1999, p. 34.
[20] H. Lagadec, C. Meis, M. Jardino, Effective potential of an rf cylindrical trap, Int. J. Mass Spectrom. Ion Processes 85 (1988) 287–299.
[21] T. Hasegawa, J.J. Bollinger, Rotating-ratio-frequency ion trap, Phys. Rev. A 72 (2005) 0434031–0434038.
[22] G. Dahlquist, A. Bjorck, Numerical Methods, Dover Publications, 2003, pp. 29–32.
[23] R.E. Mather, R.M. Waldren, J.F.J. Todd, Some operational characteristics of a quadrupole ion storage mass spectrometer having cylindrical geometry, Int. J. Mass Spectrom. Ion Phys. 33 (1980) 201–230.